Proc. Indian Acad. Sci. (Earth Planet. Sci.), Vol. 98, No. 1, April 1989, pp. 31–60.

High velocity anomaly beneath the Deccan volcanic province: Evidence from seismic tomography

H M IYER#, V K GAUR, S S RAI, D S RAMESH, C V R RAO, D SRINAGESH and K SURYAPRAKASAM

National Geophysical Research Institute, Hyderabad 500 007, India
#US Geological Survey, Menlo Park CA, USA

Abstract. Analysis of teleseismic *P*-wave residuals observed at 15 seismograph stations operated in the Deccan volcanic province (DVP) in west central India points to the existence of a large, deep anomalous region in the upper mantle where the velocity is a few per cent higher than in the surrounding region. The seismic stations were operated in three deployments together with a reference station on precambrian granite at Hyderabad and another common station at Poona. The first group of stations lay along a west-northwesterly profile from Hyderabad through Poona to Bhatsa. The second group roughly formed an L-shaped profile from Poona to Hyderabad through Dharwar and Hospet. The third group of stations lay along a northwesterly profile from Hyderabad to Dhule through Aurangabad and Latur. Relative residuals computed with respect to Hyderabad at all the stations showed two basic features: a large almost linear variation from approximately + 1 s for teleseisms from the north to – 1 s for those from the southeast at the western stations, and persistance of the pattern with diminishing magnitudes towards the east. Preliminary ray-plotting and three-dimensional inversion of the *P*-wave residual data delineate the presence of a 600 km long approximately N-S trending anomalous region of high velocity (1–4% contrast) from a depth of about 100 km in the upper mantle encompassing almost the whole width of the DVP. Inversion of *P*-wave relative residuals reveal the existence of two prominent features beneath the DVP. The first is a thick high velocity zone (1–4% faster) extending from a depth of about 100 km directly beneath most of the DVP. The second feature is a prominent low velocity region which coincides with the westernmost part of the DVP. A possible explanation for the observed coherent high velocity anomaly is that it forms the root of the lithosphere which coherently translates with the continents during plate motions, an architecture characteristic of precambrian shields. The low velocity zone appears to be related to the rift systems (anomaly 28, 65 Ma) which provided the channel for the outpouring of Deccan basalts at the close of the Cretaceous period.

Keywords. Deccan volcanic province; seismic tomography; deep structure; high velocity anomaly; teleseismic residuals; three-dimensional inversion.

1. Introduction

The Deccan volcanic province (DVP) encompasses an area of about a half million km^2 in west-central India with a possible extension of an additional 1 million km^2 beneath the Arabian Sea to the west. The Deccan basalts are primarily of tholeiitic composition with a few pockets of acidic volcanism. The volcanic flows occur as a relatively thin veneer at the surface with a thickness of 1–1·5 km in the western third of the province, thinning to about 0·4 km in the middle section and to a few meters in the eastern section (Kaila 1982). The bulk of the Deccan volcanism is now known to have occurred around 65 Ma (Mahoney 1988). About 200 Ma ago, India was wedged in the southern latitudes between Africa and Antarctica as part of the

super-continent Gondwanaland. During the Triassic period, it split off and started migrating northwards as an independent continent eventually colliding with Eurasia about 45 Ma ago. Morgan (1972) proposed that the Deccan basalts erupted during this northward migration as the sub-continent traversed over a mantle plume associated with the Reunion hot spot.

1.1 *Gravity*

The Deccan Traps lie in a broad gravity low which encompasses the whole of the south Indian shield. Within this broad low are shorter wavelength "lows" and "highs". A few of these short wavelength features have been interpreted variously: uplift and subsidence due to cycles of volcanic activity (Kailasam 1975); crustal intrusion of mafic rock (Takin 1966) and linear channels of magma flow (Qureshy 1981). We also show later that preliminary two-dimensional modelling of the gravity data indicates a lower-than-normal density in the upper mantle beneath the central part of the DVP.

1.2 *Deep seismic sounding*

Deep seismic sounding was carried out along two profiles over the Koyna region of the Deccan Traps and several others in the Saurashtra Peninsula and across the Narmada-Son lineament (Kaila *et al* 1981, 1985; Kaila 1982). Though the velocity models obtained from these profiles reflect the thickness of the surficial basalts up to 2 km, the crustal structure beneath the DVP is not significantly different from that of the precambrian south Indian shield model elsewhere as revealed by data along the Kavali-Udipi profile (Kaila 1982). Moho depth is found to vary from 39–40 km west of Koyna to 36–38 km eastwards. There is no evidence of drastic changes in the depth of major discontinuities like the Conrad discontinuity across the profile nor is there evidence of unusually high upper or lower crustal velocities which are characteristic of rift zones.

1.3 *Heat-flow*

Except for the Cambay graben where the heat-flow is somewhat higher-than-normal, other parts of the Deccan Traps show normal heat flow typical of stable continental regions (Gupta and Gaur 1984). Except for implying that the volcanic episode responsible for the Deccan volcanic flows did not leave a detectable thermal remanance in the lithosphere, the heat-flow data do not provide any information on the deep structure beneath the DVP.

In summary, the available geophysical data are inadequate to constrain a source model for the Deccan volcanism. For example, if the magmatism was caused by a mantle plume, extensive melting, differentiation and variations in physical and chemical properties of the deep structure of the lithosphere might have taken place. But the available heat-flow and deep seismic sounding data are inadequate to model the structure of the lithosphere and asthenosphere beneath the DVP which would expose alterations in structure associated with that volcanism. With this background, we designed a tomographic experiment to model in three dimensions the compressional wave velocity structure of the upper mantle beneath the DVP. Results from this experiment reveal a vast anomalous region in the upper mantle of the

DVP where the *P*-wave velocity is a few per cent higher than in the surrounding region. This is the first effort to map the deep structure beneath the DVP.

2. Tomography using teleseismic residuals

Teleseismic residuals provide an excellent approach to model the two- and three-dimensional velocity structures of the earth's crust and mantle. Numerous publications describe the use of the technique to delineate heterogeneous earth structure from global and continental scales to local scale. Recent introduction of inversion methods for teleseismic residuals (also called seismic tomography) has considerably enhanced the power of the teleseismic residual technique (Aki *et al* 1977; Humphreys and Clayton 1988). Tomographic modelling of small and large heterogeneities in the earth's crust and mantle have been carried out in diverse geologic settings (Thurber and Aki 1987; Iyer and Hitchcock 1988). The present study is the first application of this technique in India.

3. Estimation of teleseismic residuals

Teleseisms (earthquakes occurring at distances greater than approximately 20 degrees from the recording station) are recorded by a dense array of seismic stations sited over the region of interest to provide the data for tomography. The average instrument spacing in the array limits the smallest size of the velocity anomaly that can be resolved. Two-dimensional arrays yield three-dimensional models, while linear arrays yield two-dimensional models. Arrival times of the first seismic phases (P or PKIKP, PKP) are read from the seismograms and travel time from the source to the recording stations are estimated from a knowledge of the earthquake origin times. Knowing the hypocentral location of the earthquake, theoretical travel times are computed using a standard seismological table. In the present study, we used the *P*-wave travel time tables of Herrin (1968a). The travel-time residuals are simply the differences between the observed and theoretical travel times. In the mathematical notation we write,

$$R_{ij} = T^{o}_{ij} - T^{th}_{ij}$$

where, R_{ij} is the absolute residual in seconds, and T^{o}_{ij} and T^{th}_{ij} are the observed and theoretical travel times respectively at station i for event j. In addition to the information on the deep structure beneath the seismic array, R_{ij} contains effects due to errors associated with the location and origin times of the earthquakes travel-time tables, and anomalous structure at the source and along the seismic wave paths. In order to isolate the local structures from extraneous effects, relative residuals are computed independently for each event by subtracting the residual at a reference station which hopefully is located outside the anomaly under investigation from the absolute residuals at each station. Alternatively, a weighted mean of absolute residuals for each event can be used as the reference residual. Thus, the relative residual RR_{ij} for event j can be defined as,

$$RR_{ij} = R_{ij} - R_{rj},$$

where the subscript r represents the reference station, or as

$$RR_{ij} = R_{ij} - R_j,$$

where R_j represents the weighted mean of R_{ij} using all readings available for the event j. In this study all weights were chosen to be equal to unity. Consequently, R_j is a simple average of absolute residuals for the whole array.

RR_{ij} contains the information needed to model the three-dimensional relative-velocity structure beneath the seismic array. The magnitudes of the relative residuals indicate the change in velocity within the anomaly; the sign of the residuals being negative for high-velocity anomalies and vice versa. The azimuthal pattern of RR_{ij} gives an idea of the depth of the anomaly. As a rule of thumb, it may be remembered that a 10-km long anomalous ray-path in which the seismic velocity differs from the normal by 10% produces a residual of about 0·2 s.

4. Three-dimensional inversion

We have used the three-dimensional inversion technique developed by Aki *et al* (1977) (now popularly referred to as the ACH technique) to model the teleseismic residuals. Since the ACH technique is described in detail in various papers (Aki *et al* 1977; Ellsworth and Koyanagi 1977; Iyer *et al* 1981; Achauer *et al* 1986) and also its application (Aki 1982; Thurber and Aki 1987; Iyer and Hitchcock 1988), only a brief outline of the theory will be given here along the lines presented by Achauer *et al* (1986). In this technique, the volume under the array is divided into layers and each layer into a grid of rectangular blocks. An initial P-wave velocity from a known or assumed model is assigned to each layer for ray-tracing purposes. It turns out that the final results are not very sensitive to the choice of this initial velocity model. The incident wave at the bottom of the deepest layer is assumed to be plane. As it travels to the seismograph, it encounters an unknown velocity perturbation in each block. The resultant travel time delays and advances accumulated along the ray path equal the observed residual at the surface. In this treatment, the refraction of the seismic ray due to the velocity perturbation is assumed to be negligible. Thus for each ray, the following linear equation can be generated in a matrix form.

$$Am = d,$$

where A is a matrix with calculated unperturbed travel times of ray segments, m is a vector containing the unknown fractional slowness perturbations (slowness is the reciprocal of velocity), and d is a vector containing the travel time residuals. Since A^TA is near singular, Aki *et al* (1977) used the damped least-squares method to obtain the model estimate $\hat{m}$ as,

$$m = (A^TA + \theta^2 I)^{-1} A^T d,$$

where $\theta^2 = \sigma_d^2/\sigma_m^2$ is the damping parameter and σ_d^2 and σ_m^2 are the estimated variances of the data and the (unknown) true model m (Achauer *et al* 1986). It should be remembered that the estimated model contains only relative velocities, as the inputs are relative residuals.

The main drawback with the block inversion described above (resulting from finite

at it provides only a 'fuzzy' picture of the real model. The degree of 'fuzziness' on the density of instruments deployed in the seismic network, the number uthal distribution of teleseisms used and the block size. Fortunately, the east-squares inversion also produces a resolution matrix and standard errors able one to estimate the figure of merit for a computed model. The 'true' is related to the 'fuzzy' model $\hat{m}$ by the relation

$$m = R\hat{m},$$

is the resolution matrix. Each element of the symmetric singular matrix R ue between -1 and $+1$ with positive values on the diagonal. Therefore, of the matrix can be considered as an average kernel relating all of m, the el, to one block of the estimated 'fuzzy' model. Thus large diagonal elements solution matrix imply that $\hat{m}$ is a good representation of m. In general, n is good towards the middle of each layer and is rather poor near the edges. ely related to the number of ray-hits in the block. The standard errors, rom the diagonal of the covariance matrix, are indicators of the accuracy velocity perturbation. As a rule of thumb, the accuracy of individual tion estimates are about (±) 2 times the standard error for 0·8 resolution 3—4 times for 0·6 resolution (Evans 1982). When small blocks are used, the of the inversion can be assessed by looking at the whole resolution matrix ic blocks.

xperiment

ated fifteen vertical-component seismic stations (Teledyne protacorders with Hz, seismometers) in and around the southern half of the DVP (figure 1, in three consecutive deployments with Hyderabad (HYB) and Poona (POO) mmon to the whole experiment. A total of 168 teleseisms mainly from north, t, east and southeast, and in the distance range of 19 to 95 degrees were . by this network (table 2). The recorders were operated at their maximum peed of 240 mm/min and internal clocks synchronized with radio time roadcast by the National Physical Laboratory, New Delhi. Considerable taken in reading the arrival times of the first phases, thereby achieving a uracy of 0·05 s. Visual correlation of seismic waveforms and multiple readings ak, peak, zero-crossing, trough etc) were used to ensure a high relative of picks (figure 2). Despite these precautions substantial signal changes ne array led us to discard about 10% of the readings (figure 3). This as well w amplitudes of the signals also contributed to the scatter in data. Even so, magnitude of the observed relative-residuals permits us to draw significant ons.

analysis

iation *of residuals with azimuth and distance*

4—7 show the relative residuals, with respect to HYB at 13 stations plotted the respective azimuth of seismic arrivals. We used HYB as the reference

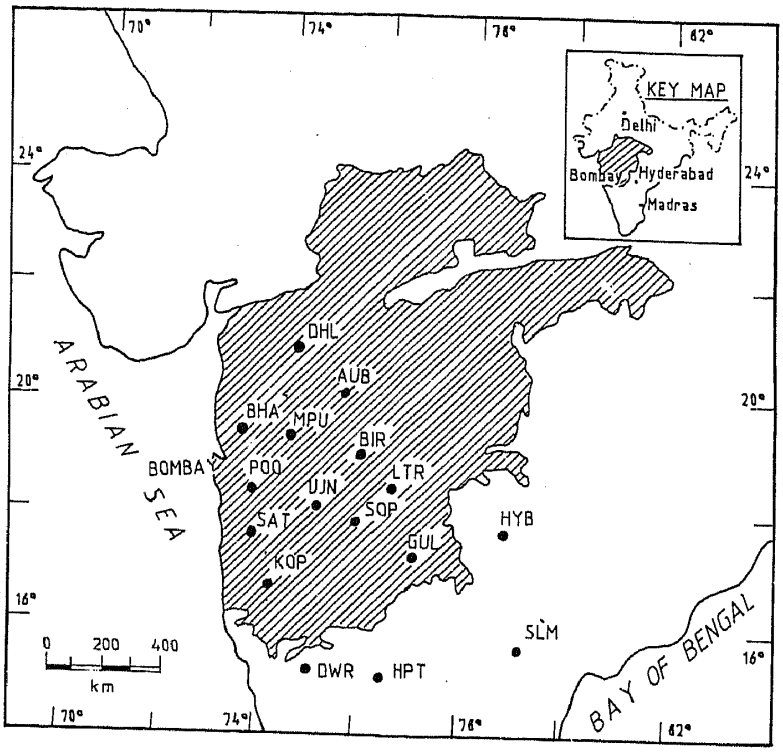

Figure 1. Map of west-central India showing the locations of seismic stations (three-letter names) used in this study. The approximate outline demarking the extension of the DVP.

Table 1. Coordinates of seismic stations.

Station name	Latitude (N)	Longitude (E)	Elevation (meters)	Duration of operation
Hyderabad (HYB)	17°25·03′	78°33·18′	510·0	Sept. 1985–Dec. 1987
Poona (POO)	18°32·84′	73°49·07′	579·3	Sept. 1985–Dec. 1987
Bhatsa (BHA)	19°31·12′	73°24·06′	185·9	Dec. 1985–Apr. 1986
Ujani (UJN)	18°04·00′	75°06·87′	496·9	Jan. 1986–Apr. 1986
Solapur (SOP)	17°38·90′	75°54·93′	475·6	Jan. 1986–May. 1986
Gulbarga (GUL)	17°19·57′	76°53·25′	470·0	Jan. 1986–Apr. 1986
Satara (SAT)	17°40·17′	74°00·19′	670·5	Jun. 1986–Feb. 1987
Kolhapur (KOP)	16°40·20′	74°15·10′	563·8	Jun. 1986–Feb. 1987
Dharwar (DWR)	15°25·27′	74°55·79′	731·5	Jun. 1986–Jan. 1987
Hospet (HPT)	15°15·31′	76°20·58′	478·5	Jun. 1986–Jan. 1987
Srisailam (SLM)	16°06·00′	78°53·50′	438·9	Jan. 1987–Mar. 1987
Aurangabad (AUB)	19°54·38′	75°18·66′	569·0	May. 1987–Dec. 1987
Bir(BIR)	18°58·37′	75°46·28′	560·0	May. 1987–Dec. 1987
Latur (LTR)	18°21·25′	76°33·75′	610·0	May. 1987–Dec. 1987
Dhule (DHL)	20°55·49′	74°47·01′	265·0	Jun. 1987–Dec. 1987

Table 2. List of teleseisms used in this study which provided readings in at least 3 stations.

Sl. No.	Source region	Origin time	Depth (km)	Coordinates	
1.	MOLUCAzc(01/03/86)	09·43·28·6	39	00:58·32S	126:52·08E
2.	AFGHAN(01/14/86)	03·03·37·4	245	36:20·46N	71:01·44E
3.	HONSHUzc(01/16/86)	08·34·43·7	436	29:48·12N	138:39·72E

(*continued*)

Table 2. (*continued*)

Sl. No.	Source region	Origin time	Depth (km)	Coordinates	
4.	MINDROzc(01/16/86)	15·45·06·7	223	13:41·10N	120:49·32E
5.	ALUTINtr(01/18/86)	01·59·01·6	33	51:33·18N	173:06·54W
6.	MOLUCAtr(01/22/86)	14·57·13·0	59	00:28·02S	124:21·96E
7.	HOKADOtr(01/31/86)	17·48·04·4	69	42:13·68N	142:59·76E
8.	CELBEStr(02/01/86)	15·00·35·8	392	02:54·36N	124:04·50E
9.	VANATUzc(02/02/86)	01·44·05·4	31	13:37·56S	166:41·58E
10.	BONINtr(02/03/86)	20·47·35·3	508	27:47·46N	139:33·12E
11.	HINDKUzc(02/04/86)	19·43·56·6	203	36:25·56N	70:41·76E
12.	AFGHANpk(02/11/86)	07·14·24·2	119	36:22·32N	70:54·60E
13.	HONSHUpk(02/12/86)	02·59·30·4	30	36:23·04N	141:07·68E
14.	PAPNGUzc(02/12/86)	11·27·45·4	34	06:32·16S	147:25·98E
15.	HALMHApk(02/12/86)	23·02·12·8	135	01:36·24N	127:18·30E
16.	CARSBRzc(02/15/86)	19·56·35·9	10	04:24·72N	62:42·24E
17.	KURILEpk(02/19/86)	10·54·46·2	115	48:34·74N	153:24·90E
18.	PHLPNEzc(02/19/86)	11·40·27·5	77	18:56·70N	121:18·24E
19.	AUSTLAzc(02/24/86)	01·26·58·2	32	12:45·24S	114:36·54E
20.	HALMHApk(02/24/86)	02·31·26·7	118	01:43·74N	127:21·24E
21.	BANDCApk(03/01/86)	16·41·40·6	80	06:18·00S	130:56·94E
22.	KAMCHK(03/02/86)	03·14·41·8	118	51:40·68N	156:56·16E
23.	SOLMONzc(03/06/86)	12·31·24·0	72	07:00·00S	155:46·86E
24.	NEWBRTfb(03/07/86)	02·46·52·0	116	04:59·40S	151:42·60E
25.	HANDUKzc(03/11/86)	23·07·38·2	206	36:28·92N	70:39·60E
26.	BONINzc(03/17/86)	09·18·25·2	476	27:25·26N	139:51·96E
27.	FLOREStr(03/21/86)	21·35·35·8	614	07:27·30S	120:38·76E
28.	HONSHUtr(03/25/86)	04·00·43·3	144	37:15·72N	139:25·38E
29.	BRAZILzc(03/26/86)	22·06·57·6	609	07:07·50S	71:38·28W
30.	NBRTANzc(04/03/86)	07·39·53·9	30	06:20·40S	151:42·90E
31.	KURILEzc(04/05/86)	22·59·09·4	80	44·27·96N	147:51·42E
32.	MINDNOtr(04/09/86)	21·56·19·6	56	09:58·14N	126:09·24E
33.	MOLUCAzc(04/10/86)	02·21·13·3	33	00:58·14S	126:50·28E
34.	MARANAzc(04/13/86)	03·00·20·9	304	17:11·28N	145:37·26E
35.	VANATUzc(04/14/86)	00·25·12·4	33	13:56·76S	166:58·62E
36.	KURILEzc(04/16/86)	12·52·19·7	52	43:52·98N	147:33·96E
37.	TANMBRzc(04/18/86)	08·08·39·2	44	06:00·42S	131:32·82E
38.	WIRIANzc(04/20/86)	07·03·30·8	33	02:22·50S	139:19·08E
39.	CRETE tr(04/27/86)	09·27·02·3	10	34:38·46N	23:24·42E
40.	SUMTRAzc(04/29/86)	13·59·21·8	47	04:24·00N	95:00·24E
41.	RYUKYUtr(04/30/86)	23·14·43·7	44	28:42·66N	130:02·82E
42.	PAPUAGzc(06/24/86)	03·11·30·9	102	04:26·88S	143:56·58E
43.	FLOREStr(06/27/86)	03·09·50·8	229	07:56·82S	122:47·46E
44.	FLORESpk(06/27/86)	03·09·50·8	229	07:56·82S	122:47·46E
45.	TAGYKApk(06/29/86)	21·47·59·6	20	05:20·16S	20:32·34E
46.	MEXICOpk(07/05/86)	22·09·36·9	112	15:28·02N	92:34·92W
47.	CARBRGfb(07/07/86)	16·26·56·6	8	10:23·34N	56:49·92E
48.	MINAHAzc(07/08/86)	04·27·34·6	245	01:59·82N	124:18·30E
49.	MOLUCApk(07/09/86)	23·10·53·1	28	01:54·24N	126:31·50E
50.	SIRANfb(07/12/86)	07·54·26·8	10	29:57·72N	51:34·92E

(*continued*)

Table 2. (*continued*)

Sl. No.	Source region	Origin time	Depth (km)	Coordinates	
51.	AFUSSRzc(07/17/86)	15·46·37·0	47	36:40·08N	71:14·82E
52.	FOXIS zc(07/19/86)	04·31·55·9	33	53:21·12N	165:52·92W
53.	KURILEzc(07/19/86)	05·59·36·2	141	47:15·84N	151:07·62E
54.	BURMAtr(07/26/86)	20·24·47·8	27	23:45·18N	94:10·62E
55.	EUSSRpk(07/26/86)	14·46·18·9	310	45:25·32N	137:04·20E
56.	CHINApk(08/06/86)	19·55·15·6	34	29:20·64N	100:54·90W
57.	PHILPNzc(08/09/86)	00·53·12·6	80	14:05·94N	120:20·10E
58.	HALMRAzc(08/10/86)	04·40·49·7	104	01:59·10N	128:16·26E
59.	MOLUCAtr(08/17/86)	15·27·41·2	31	02:16·56N	126:57·54E
60.	BANDASzc(08/19/86)	12·52·41·1	33	04:07:32S	129:19·44E
61.	PHILPNzc(08/19/86)	22·41·35·8	98	12:30·84N	124:28·68E
62.	SIOCENtr(08/20/86)	21·15·46·4	10	01:58·38S	87:05·28E
63.	ROMANAzc(08/30/86)	21·28·35·4	132	45:32.82N	26:18·86E
64.	VOLCNOpk(08/31/86)	09·23·04·7	46	23:02·52N	144:07·20E
65.	KURILEtr(09/01/86)	21·47·35·0	148	46:37·86N	150:00·60E
66.	HALMRAzc(09/09/86)	15·58·22·5	33	00:55·62N	127:56·64E
67.	NBRTANtr(09/11/86)	00·18·25·5	51	05:11·22S	152:26·52E
68.	MOLUCAtr(09/11/86)	17·54·03·0	33	00:28·44N	125:51·72E
69.	HINDKUtr(09/13/86)	14·14·54·3	200	36:26·52N	70:45·96E
70.	SOLMONzc(09/14/86)	20·58·23·1	59	06:28·20S	154:54·96E
71.	ANDREOtr(09/15/86)	06·29·35·8	33	51:33·66N	177:05·10W
72.	MARINAtr(09/16/86)	18·20·17·7	48	19:22·56N	146:18·06E
73.	AFUSSRzc(09/17/86)	12·08·09·4	120	37:17·40N	71:43·80E
74.	AFUSSRtr(09/17/86)	12·08·09·4	120	37:17·40N	71:43·80E
75.	CARBRGfb(09/17/86)	21·25·15·0	10	10:29·82N	56:59·98E
76.	HONSHUzc(09/20/86)	03·04·58·7	75	36:27·24N	140:31·20E
77.	BANDAzc(09/22/86)	16·15·05·8	123	06:42·96S	130:25·62E
78.	BONINzc(09/27/86)	19·38·42·1	30	27:52·02N	142:46·62E
79.	BANDASzc(10/01/86)	13·00·06·3	343	05:34·74S	128:37·02E
80.	MEDRNSpk(10/02/86)	10·12·45·6	46	34:50·76N	28:18·84W
81.	HALMRAtr(10/04/86)	02·00·08·0	106	02:58·92N	128:02·16E
82.	ANDREOzc(10/06/86)	04·21·46·7	43	51:51·78N	176:15·42W
83.	SHONSUtr(10/07/86)	11·40·55·0	400	31:54·42N	137:40·56E
84.	JAVARzc(10/10/86)	17·48·24·6	82	07:29·88S	107:13·98E
85.	HINDKUtr(10/13/86)	16·11·40·4	117	36:04·02N	70:50·88E
86.	HINDKUzc(10/13/86)	16·11·40·4	117	36:04·02N	70:50·88E
87.	HONSHUtr(10/13/86)	21·17·50·9	65	37:06·12N	141:00·66E
88.	BANDASzc(10/17/86)	07·32·51·3	67	05:16·32S	131:25·92E
89.	ANDREOpk(10/18/86)	01·02·52·1	33	51:43·80N	175:17·10W
90.	JAVAzc(10/18/86)	22·09·31·7	643	05:37·86S	109:59·82E
91.	HALMRApk(10/21/86)	21·57·59·4	142	01:32·46N	127:25·44E
92.	SACRUZtr(10/22/86)	08·59·28·8	165	10:34·14S	166:02·40E
93.	EPGNEAzc(10/23/86)	03·54·20·8	127	06:05·82S	146:18·36E
94.	NCHILEpk(10/24/86)	02·42·51·6	51	25:19·14S	70:10·56W
95.	NCHILEzc(10/24/86)	02·42·51·6	51	25:19·14S	70:10·56W
96.	AIRISEpk(10/28/86)	15·11·23·3	10	30:28·26S	60:10·92E
97.	MINDNOfb(10/29/86)	20·11·39·7	72	05:43·32N	125:19·86E

(*continued*)

Table 2. (*continued*)

Sl. No.	Source region	Origin time	Depth (km)	Coordinates	
98.	MINDNOzc(10/29/86)	20·11·39·7	72	05:43·32N	125:19·86E
99.	BURMAzc(11/01/86)	05·02·42·4	26	26:54·12N	96:25·50E
100.	MINDNOzc(11/06/86)	02·48·23·6	62	09:00·42N	126:14·40E
101.	ANDREOzc(11/06/86)	18·27·00·1	33	51:28·14N	176:41·04W
102.	MOLUCAfb(11/11/86)	00·02·32·0	79	02:24·84N	126:48·66E
103.	MOLUCAzc(11/11/86)	00·02·32·0	79	02:24·84N	126:48·66E
104.	TAKXJGfb(11/12/86)	10·06·15·3	115	38:27·30N	73:16·68E
105.	TAKXJGzc(11/12/86)	10·06·15·3	115	38:27·30N	73:16·68E
106.	TAIWANtr(11/14/86)	21·20·10·5	34	23:54·06N	121:34·44E
107.	TAIWANzc(11/14/86)	23·04·37·0	33	23:51·96N	121:42·66E
108.	PRUECQfb(11/23/86)	01·39·23·9	106	03:20·52S	77:24·66W
109.	PRUECQzc(11/23/86)	01·39·23·9	106	03:20·52S	77:24·66W
110.	HJAPANzc(11/28/86)	22·29·35·1	41	36:20·70N	141:10·44E
111.	HPAJANpk(11/30/86)	20·15·30·3	37	38:51·18N	141:56·88E
112.	NIBRISpk(12/07/86)	05·40·39·2	215	06:46·98N	95:07·20E
113.	SOLMISfb(12/11/86)	19·56·12·5	61	10:29·28S	160:42·90E
114.	HJAPANfb(12/14/86)	00·11·31·2	352	32:43·62N	137:43·38E
115.	AFUSSRzc(12/17/86)	08·31·30·3	225	36:32·34N	71:07·50E
116.	AFUSSRzc(12/18/86)	07·23·30·0	182	36:34·08N	71:21·18E
117.	ANDREOfb(12/19/86)	13·50·10·3	33	51:31·02N	176:58·62W
118.	ANDREOtr(12/19/86)	13·50·10·3	33	51:31·02N	176:58·62W
119.	TAIWANzc(12/21/86)	02·42·49·0	275	25:31·02N	121:30·42E
120.	MARINAtr(01/01/87)	16·25·34·1	74	02:42·90S	138:21·78E
121.	MARINAzc(01/01/87)	16·25·34·1	74	02:42·90S	138:21·78E
122.	CHINAzc(01/05/87)	22·52·46·5	17	41:57·84N	81:19·14E
123.	TAIWANfb(01/06/87)	05·07·48·1	38	23:58·56N	121:43·74E
124.	TAIWANzc(01/06/87)	05·07·48·1	38	23:58·56N	121:43·74E
125.	NIRELRfb(01/08/87)	19·48·55·4	44	04:44·16S	153:06·30E
126.	NIRELRzc(01/08/87)	19·48·55·4	44	04:44·16S	153:06·30E
127.	HONSHUzc(01/09/87)	06·14·44·8	68	39:53·70N	141:40·62E
128.	HOKKAIzc(01/14/87)	11·03·48·7	102	42:33·90N	142:51·00E
129.	KAMCHTzc(01/19/87)	06·47·43·0	42	54:44·64N	163:16·62E
130.	NEPALzc(01/19/87)	07·46·24·4	33	28:23·10N	83:40·92E
131.	NEPALzc(01/19/87)	08·12·05·8	33	28:14·58N	83:34·32E
132.	MARINAzc(01/21/87)	11·26·36·6	118	20:36·48N	144:53·10E
133.	MOLUCAfb(01/23/87)	17·51·09·2	72	01:38·76N	126:31·86E
134.	MOLUCAzc(01/23/87)	17·51·09·2	72	01:38·76N	126:31·86E
135.	HINDKUtr(05/05/87)	15·40·47·5	208	36:28·80N	70:40·38E
136.	KAZAKHzc(05/06/87)	04·02·05·6	1	49:49·80N	78:07·50E
137.	ANDREOzc(05/06/87)	04·06·14·1	20	51:16·32N	179:53·88W
138.	NBRITNzc(05/06/87)	12·39·49·1	20	05:42·90S	152:39·36E
139.	EUSSRzc(05/07/87)	03·05·49·1	430	46:44·16N	139:13·92E
140.	BALIStr(05/10/87)	00·37·10·0	42	07:44·22S	115:59·82E
141.	TALAUDzc(05/11/87)	09·59·34·1	94	04:28·20N	127:42·54E
142.	MINDNOzc(05/12/87)	01·30·25·0	25	07:05·40N	126:42·06E
143.	ICELNDzc(05/25/87)	11·31·54·3	8	63:51·00N	19:43·68W
144.	BANDASzc(05/30/87)	16·54·04·7	138	06:03·84S	130:31·08E

(*continued*)

Table 2. (*continued*)

Sl. No.	Source region	Origin time	Depth (km)	Coordinates	
145.	KURILEzc(05/30/87)	17·19·00·1	53	44:40·14N	150:17·34E
146.	MINHSAzc(05/31/87)	18·32·17·0	79	00:44·88N	121:56·46E
147.	ANDREOzc(06/01/87)	00·15·14·3	33	51:32·40N	177:30·54W
148.	CHINAzc(06/05/87)	04·59·58·3	1	41:35·04N	88:44·22E
149.	PHILIPtr(06/05/87)	21·25·11·2	45	05:22·86N	127:32·04E
150.	PHILIPtr(06/05/87)	22·00·03·1	47	05:15·90N	127:30.78E
151.	PHILIPzc(06/07/87)	05·49·43·6	15	20:25·74N	121:21·96E
152.	KURILEfb(06/13/87)	14·00·39·3	42	44:40·26N	150:23·52E
153.	TALAUDtr(06/15/87)	06·31·44·7	136	03:54·94N	125:56·94E
154.	KAZAKHzc(06/20/87)	00·53·04·8	1	49:54·78N	78:44·10E
155.	IRIANtr(06/27/87)	00·17·04·6	21	02:09·84S	138:10·20E
156.	KYUSHUzc(07/03/87)	10·10·43·7	168	31:11·76N	130:19·32E
157.	CHAGOStr(07/03/87)	18·03·59·7	26	06:47·16S	72:14·82E
158.	ALEUTNpk(07/05/87)	09·23·00·0	33	51:29·16N	174:39·60E
159.	ALEUTNpk(07/06/87)	00·03·25·6	33	51:30·48N	174:43·26E
160.	TALAUDpk(07/07/87)	10·36·03·7	70	05:24·18N	125:01·68E
161.	KURILEzc(07/08/87)	22·56·02·7	152	46:26·22N	149:33·48E
162.	TALAUDzc(07/14/87)	04·31·23·0	33	03:50·04N	126:32·52E
163.	OKHTSKzc(07/14/87)	23·46·03·5	591	49:37·86N	147:49·68E
164.	HONSHUtr(07/16/87)	05·46·29·5	310	33:03·54N	138:05·76E
165.	KAZAKHpk(07/17/87)	01·17·07·0	1	49:47·94N	78:06·60E
166.	TALAUDtr(07/22/87)	08·03·17·2	51	04:03·06N	125:34·92E
167.	MINHASfb(07/31/87)	00·27·32·0	167	00:10·50N	123:36·30E
168.	KAZAKHzc(08/02/87)	00·58·06·8	1	49:52·80N	78:55·02E

Note: Code after event name indicates pick: fb, first break; zc, zero crossing; pk peak; tr, trough. There are a few multiple readings in the data set.

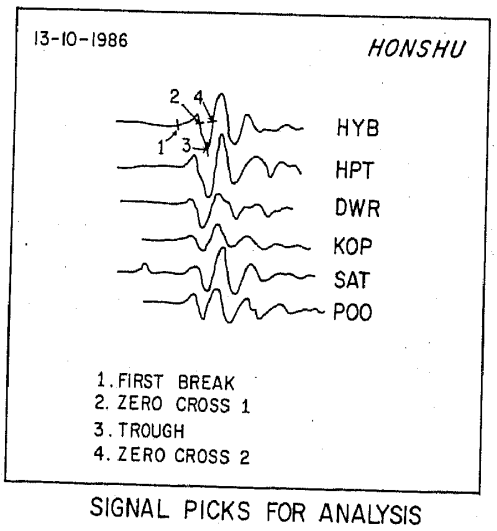

Figure 2. Seismograms showing how arrival-time are made.

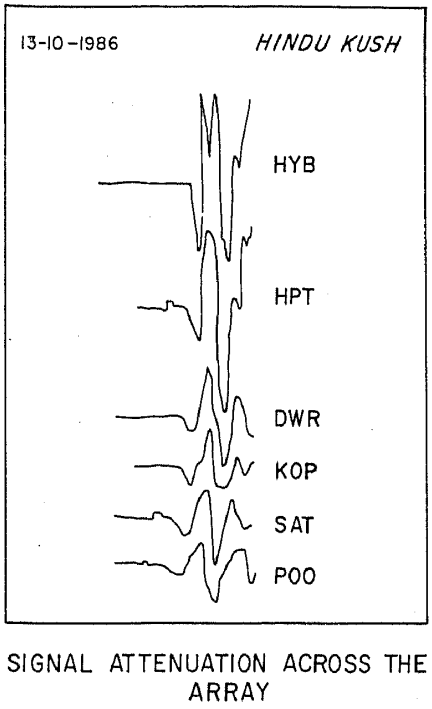

Figure 3. Signal attenuation and signal-shape changes observed at some of the stations.

station because of its location on Precambrian granite outside the DVP. A comparison of residuals at HYB with those at Srisailam—a station also on Precambrian granite about 150 km south-southeast of HYB—supports our assumptions that stations on the Precambrian granite are "normal" compared to those over the Deccan basalts.

For each station, the data were grouped into four categories according to epicentral distances: all distances, closer than 30°, 30° to 70° and beyond 70°. We first examine the data from Poona (POO) where the largest data set is available (figure 4). Note that the range of variation of residuals is about 2 s varying from 1 s in the north to −1 s in the east (figure 4a). The relative residuals also depend on the epicentral distance and which determines the angle of emergence at the seismic station. Observe that for distances $<30°$ the relative residuals are mostly positive (about +1 s) for all azimuths (figure 4b), with strong azimuthal variation occurring in the 30° to 70° range (figure 4c) and a less pronounced but still clear variation occurring for distances $>70°$ (figure 4d). Comparison of the relative residuals along the east-southeasterly profile from BHA, the westernmost station, to GUL on the eastern margin of DVP shows the pattern of residuals at BHA to be quite similar to that at POO but with larger variations from +1·5 s to −1·8 s (figure 5). Relative residuals at UJN, SOP and GUL show a similar azimuthal variation, but with a progressive decrease in magnitude towards HYB (figure 5). GUL, closest to HYB, shows the smallest residuals and is a key station to substantiate our argument that the strong azimuthal variation observed at other stations are associated with some anomaly in the deep structure beneath the DVP. The relative residuals along the southeasterly profile from DHL to AUB, BIR and LTR (figure 6) also show a decreasing azimuthal variation towards the eastern margin of the DVP, though LTR has five strong negative residuals in the 40–100° azimuth range and 30–70° distance range, cautioning against simplified inferences. Note that the residuals at these stations for distances $<30°$ are generally negative,

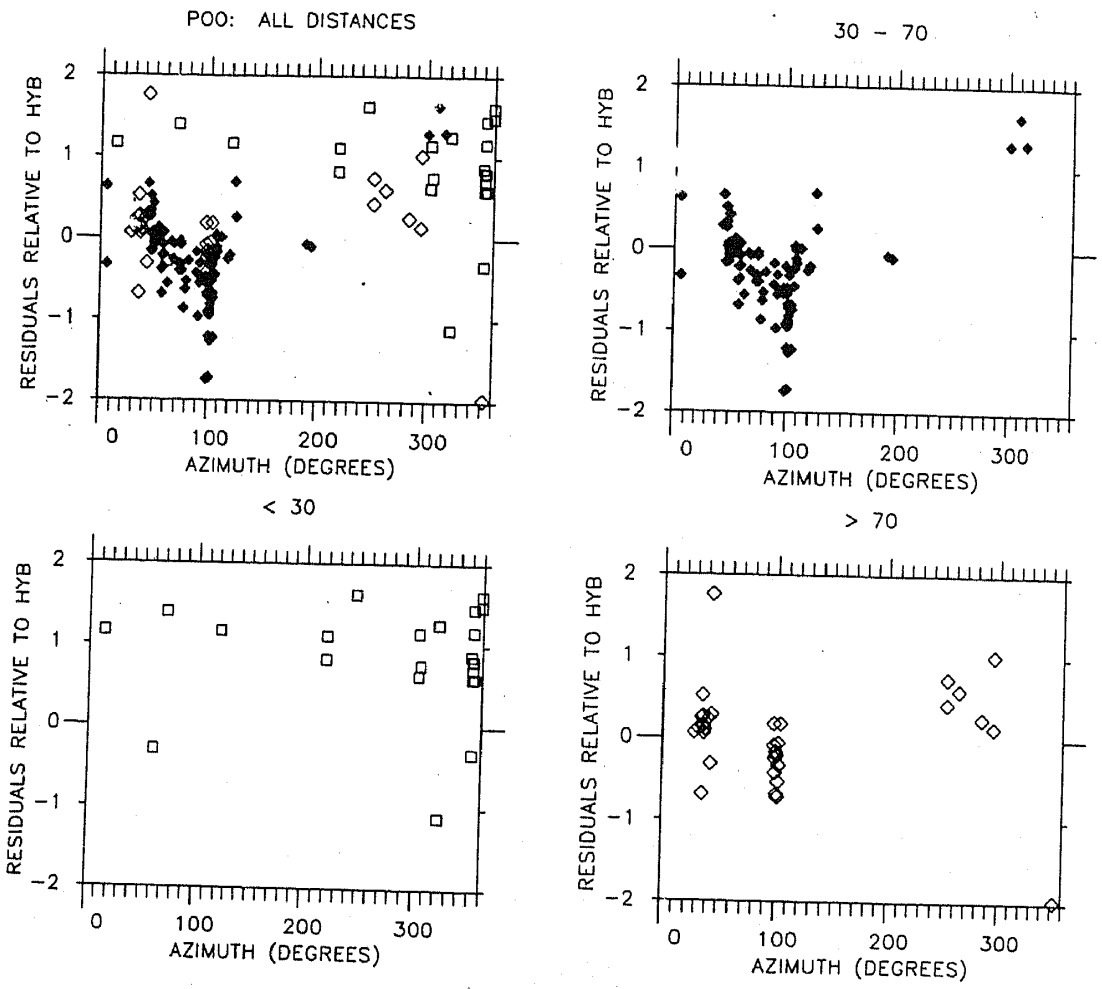

Figure 4. Relative residuals at POO with respect to HYB plotted as a function of azimuth of arrival. (**a**) All distances; hollow squares represent events at distances $<30°$; solid diamonds represent events in the distance range of 30–70°; hollow diamonds represent events at distances $>70°$. (**b**) Events at distances $<30°$. (**c**) Events in the distance range 30–70°. (**d**) Events at distances $>70°$.

unlike those observed at other stations. The southerly profile, comprised of stations SAT, KOP and DWR (figure 7) shows a behaviour similar to BHA and POO (figures 4 and 5). One surprise is at the southernmost station HPT (figure 7), south of GUL (figure 5) but outside the DVP. This station behaves similar to the western stations implying that the velocity anomaly responsible for the observed azimuthal variations extends even outside the DVP to the southeast.

Note the abrupt transition of residuals from negative values to positive near the 100° azimuth range observed at all stations in the experimental area. In order to test whether this feature in the azimuthal pattern of residuals could be due to a positive residual bias at HYB, we examined the relative residual patterns using the average event residual as reference and found that no such bias exists. The relative residuals thus calculated retained this feature at all these stations including Hyderabad, implying that it could not have arisen from any fortuitous cause related to the choice of Hyderabad as a reference station. We feel that this sharp transition in the residual patterns reflects a sharp velocity transition in the upper mantle outside the region being modelled.

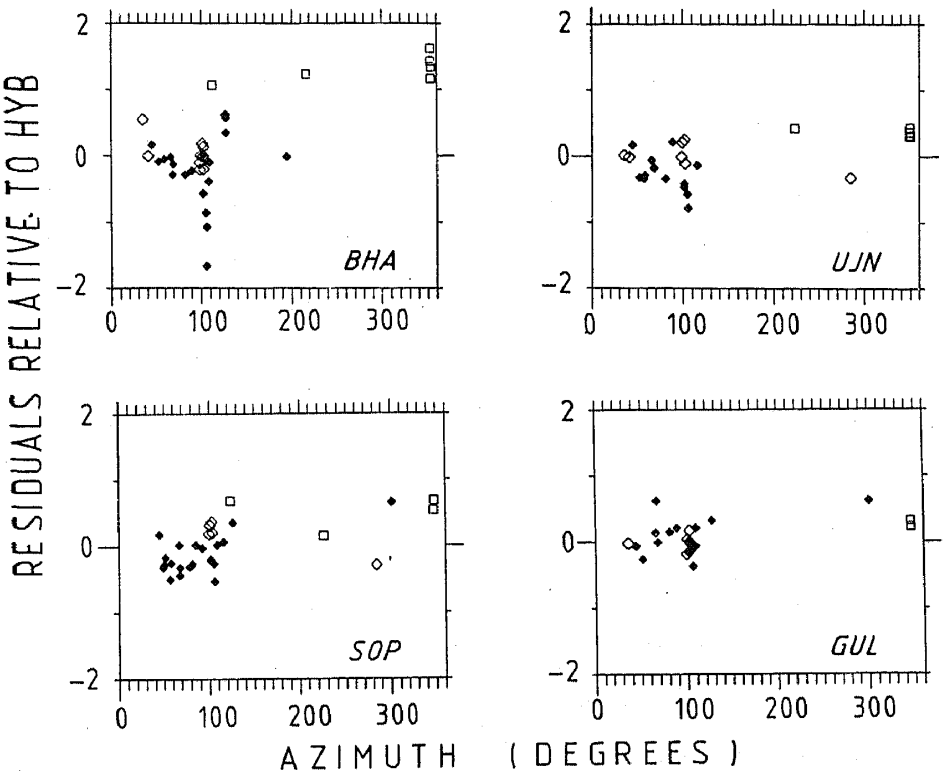

Figure 5. Relative residuals at BHA, UJN, SOP and GUL.

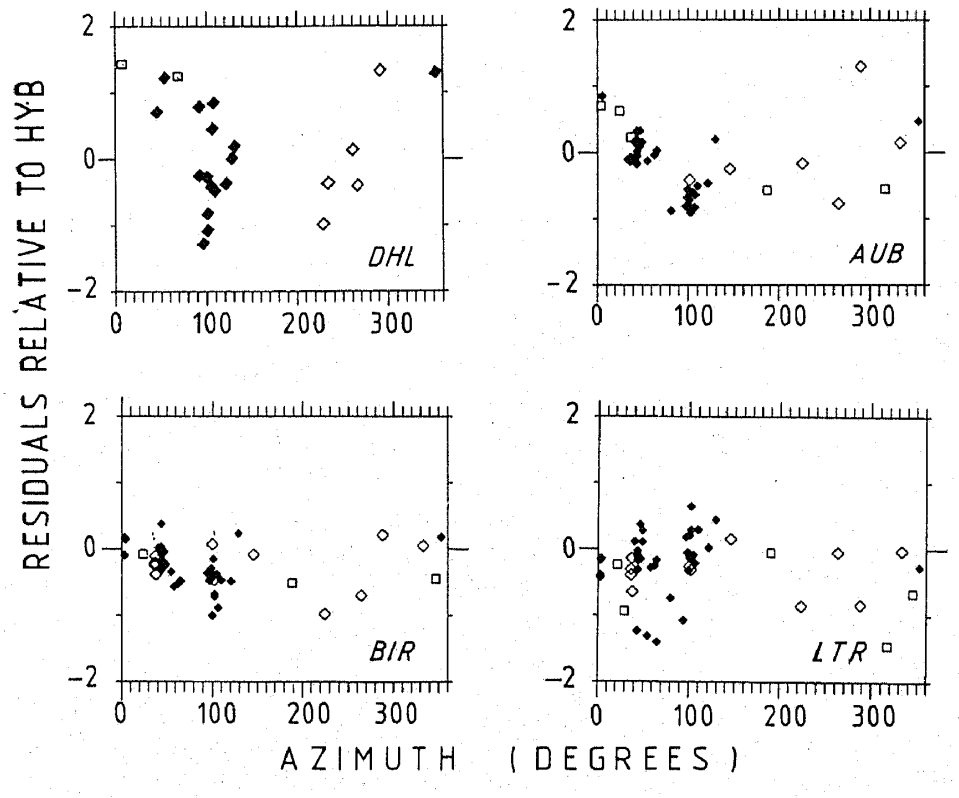

Figure 6. Relative residuals at DHL, BIR and LTR.

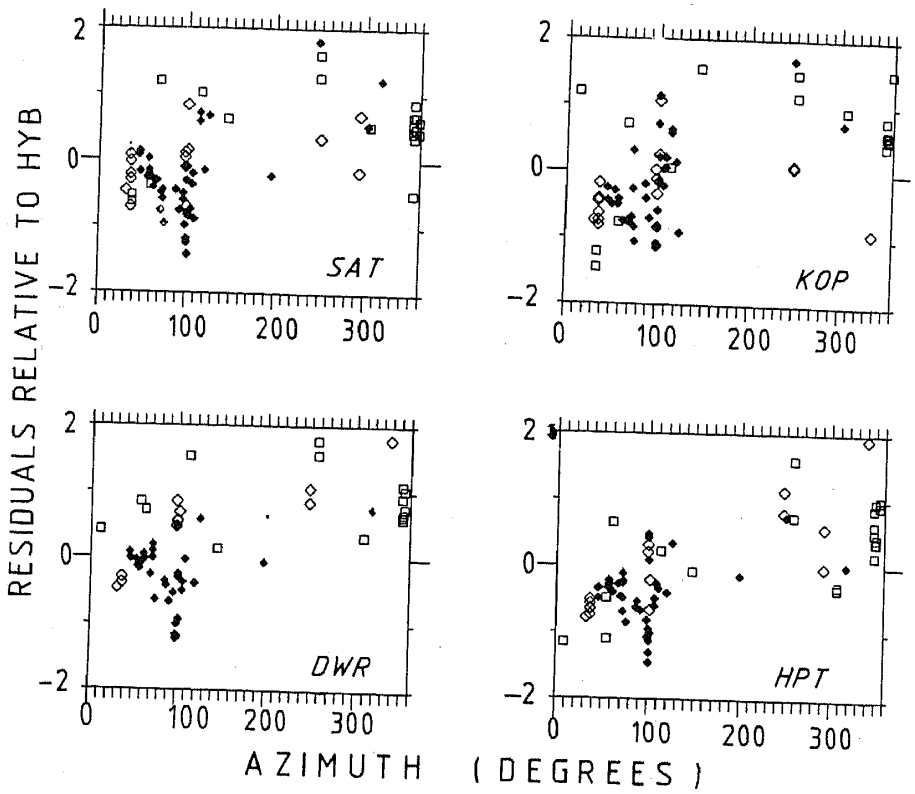

Figure 7. Relative residuals at SAT, KOP, DWR and HPT.

7. Analysis using the simple ray plotting technique

In this section we use simple ray-plotting techniques to show that the azimuthal and spatial variation of the relative residuals discussed above can be explained only in terms of velocity perturbations in the upper mantle of the DVP region. But first we evaluate the possible contributions that surficial and crustal layers can make to the residuals.

Variation in the thickness of basalt cover which attains a maximum of about 2 km in the western part, can given rise to a maximum relative residual of +0·04 s assuming the *P*-wave velocity of the Deccan basalts and the basement rock to be 4·8 km/s and 6·0 km/s respectively (Kaila 1981; Kaila 1982). Further, even a 1·0 km thick low-velocity sedimentary layer with a velocity of 4·0 km/s underlying the Deccan Traps, such as that found by Kaila *et al* (1981) in the Saurashtra Peninsula, will contribute a residual of less than 0·1 s. This is even lower than the noise level in our experiment.

7.1 *Effect of the variation of crustal thickness*

The sub-trappean crustal model in the Koyna area of Deccan basalts has been approximated by three layers of 10, 15 and 15 km thickness with average velocities of 5·7, 6·5 and 7·0 km/s respectively (Kaila *et al* 1982). Variation in the thickness of any of these layers by as much as 5 km will give rise to a total residual of only about 0·1 s. Crustal models of the Koyna region show that its thickness varies from 31·5 km near the coast to 39 km near Koyna (Kaila 1982). Even if we take the velocity contrast

across the Moho to be about 1·0 km/s this order of variation in crustal thickness will only cause the arrivals to be 0·2 s earlier at the western stations compared with those at the eastern stations. The effect is approximately the same if the thinning of the crust is distributed over all the three layers.

It is thus clear that possible variations in the thicknesses of basalts, and sub-trappean sedimentary layers, if present, as well as those of the upper or of the whole crust can at the most account for only +0·2 s of the observed spatial variation of the relative residuals. The azimuthal variation cannot be accounted for by such shallow features at all. We therefore conclude that most of the observed residual pattern can only be accounted for by deep upper mantle features.

7.2 *Ray plotting analysis*

To delineate qualitatively the zones of anomalous velocity structure responsible for the large azimuthally varying observed residuals, we first used a simple ray-tracing procedure similar to that used by Iyer *et al* (1981). From a knowledge of the emergent angles of seismic rays at various stations, inferred from the depth and epicentral distances of the respective teleseisms, rays are projected backwards from the various stations for each teleseism. The corresponding relative residuals are then projected on flat layers at three different depths (100, 200 and 300 km). If the observed residuals are due to the presence of an anomalous body rather than a random velocity perturbation, the whole set of projected residuals would be expected to show coherent signs and magnitudes so that they can be contoured when the depth chosen for the projection is correct. After considerable experimentation using data corresponding to $\Delta > 30°$, we found that the maximum coherence was achieved for projection at a depth of 200 km. Also, some form of subjective averaging was needed to reduce too many overlapping numbers. Figure 8 shows the result of this projection to 200 km depth using the above constraints. The main inference from this figure is that it outlines, albeit broadly, a 200-km wide north-south trending region of negative residuals of magnitude >0·5 s extending from AUB in the north and probably continuing south beyond HPT. Since better constraints on the region of anomalous high velocity is provided by inversion of residuals which is presented below, we do not want to overinterpret this rather crude modelling of our data. However, we would like to state that this analysis, though not providing adequate constraints to delineate the anomalous structure beneath the Deccan Traps, suggests that the observed residuals are best interpreted in terms of a heterogeneous structure in the upper mantle consisting of higher-than-normal velocities beneath the south-central part of the DVP and lower-than-normal velocities in the west-central part.

8. Tomographic results

Ideally, to obtain well-constrained tomographic models, we need a set of teleseismic arrivals from events that are fairly well-distributed in various azimuths and distance ranges. Further, the arrival-time readings should be of high quality with minimal scatter, and the data set should be homogeneous and simultaneous at all stations in the seismic network. Though our experiment does not satisfy any of these criteria strictly, the similarity of inverted models for varying block and layer configurations,

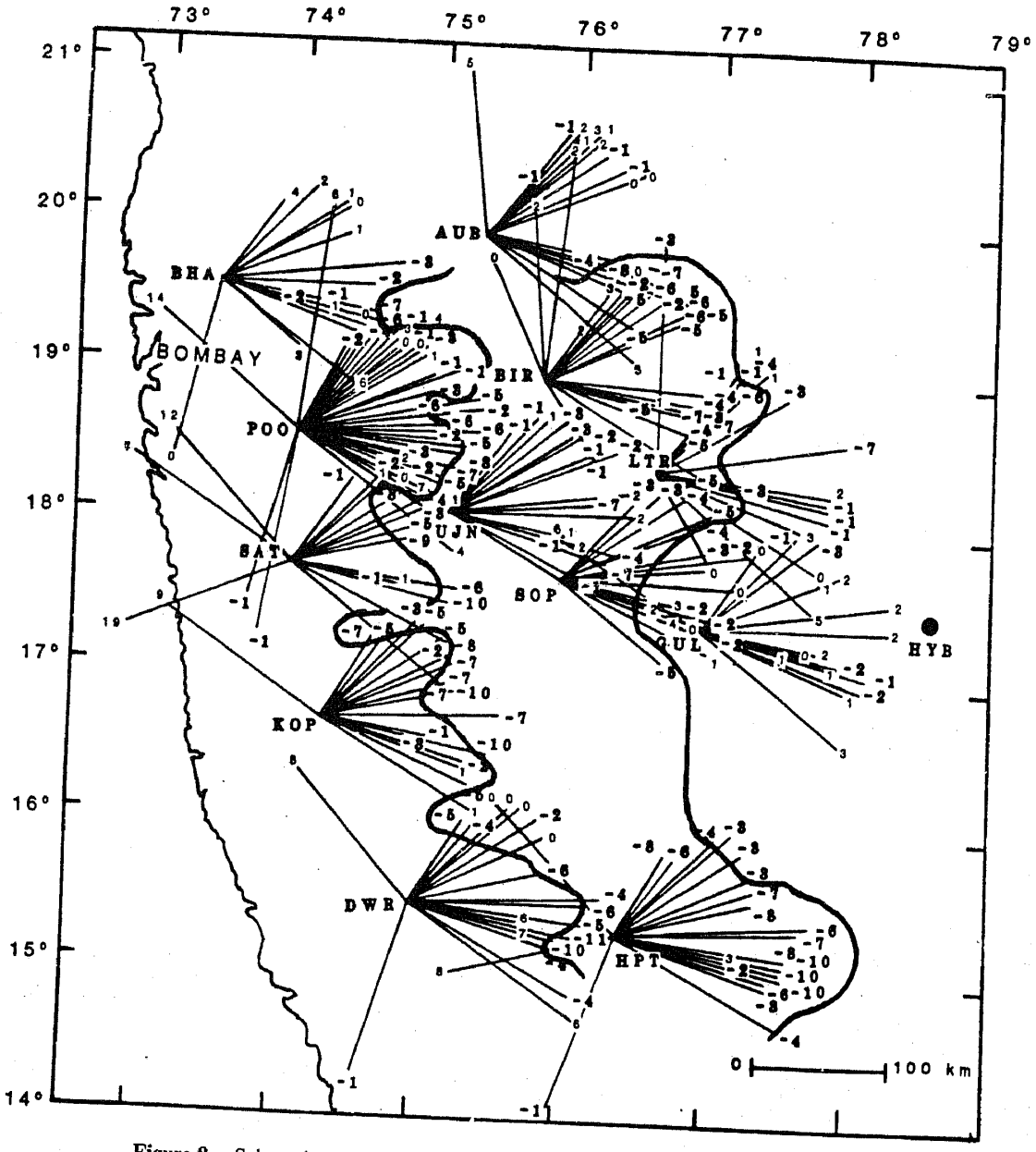

Figure 8. Selected averaged relative residuals projected at 200-km depth.

suggests that they correctly resolve first-order features of the anomalous three-dimensional *P*-velocity structure beneath the DVP. Also, these models agree with the qualitative inference derived from the azimuthal patterns of residuals using the ray-plotting approach discussed above. We performed numerous ACH inversions for a variety of layered models. The dimensions of the block were 200 km in the east-west direction and 150 km in the north-south direction. We use mantle velocities from Herrin's (1968b) earth model and the crustal velocity of 6·45 km/s (Kaila 1982). For each inversion the respective resolution matrix and standard errors were studied with a view to assessing the figure of merit of the solution. Note that ACH inversions use relative residuals based on the average of all available readings over the network for each event. Hence no specific reference stations were used.

9. Models

Although a large number of models were used for inversion, description of a few of these models together with the corresponding data variance improvements are given in table 3. The main feature of the models, that is an anomalous high-velocity zone, appears to be significant only at sub-crustal depths. In order to constrain the upper boundary of the anomalous zone, we first analyse a series of two-layer models using all available data. These are shown in figure 9. The numbers indicate velocity perturbations, positive numbers denoting higher-than-normal velocities and negative numbers

Table 3. Description of models.

No. of Layers	Layer thicknesses (km)	Variance improvement (%)
2	40, 60	16·0
2	40, 160	27·0
2	40 260	30·0
2	40, 360	31·0
3	100, 300, 200	53·0
3	150, 250, 200	63·0
4	40, 160, 200, 200	46·0

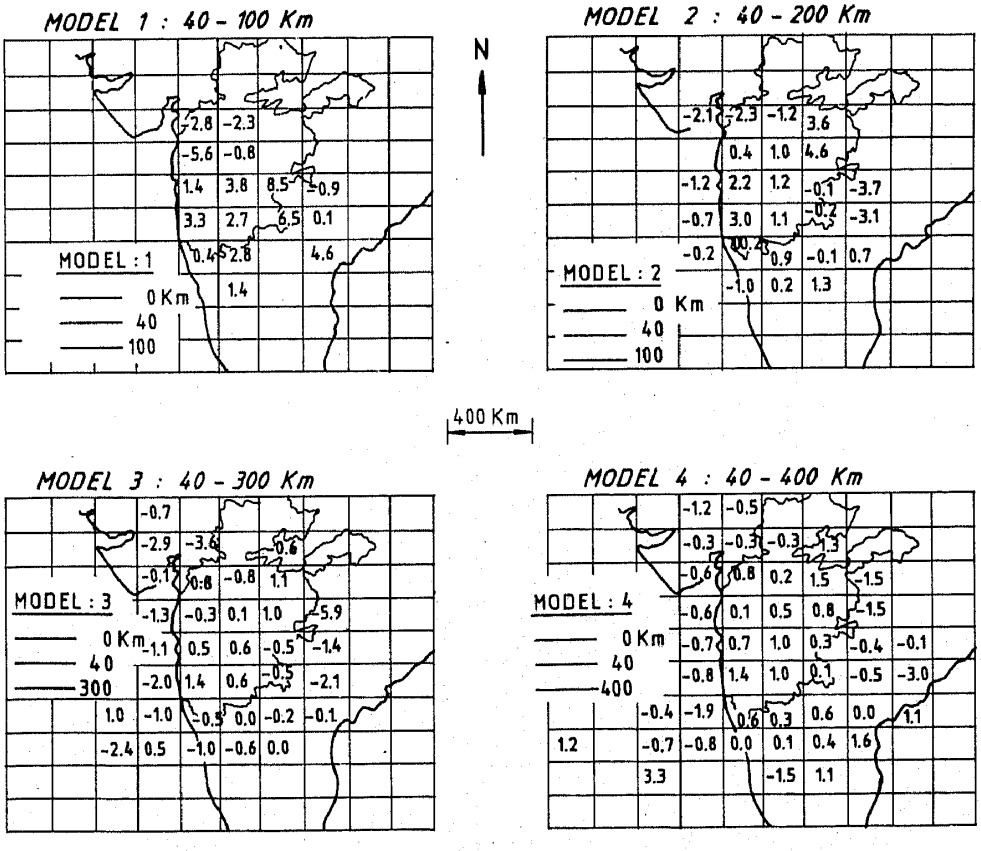

Figure 9. Second layer of 2-layer tomographic models derived using data at all available distances. Numbers indicate percentage velocity perturbations.

indicating lower-than-normal velocities. Note that all these models invariably show the presence of a high velocity region within the DVP surrounded by a relatively low velocity region. The magnitude and lateral extent of the velocity perturbations vary with the model. Although the anomalies are reflected in all the models presented below, the first one with a layer thickness of 40–100 km shows only a small variance improvement (16%) compared with others whose variance improvement ranges from 26–32%, suggesting that the high velocity anomaly (upto 4%) is confined to a depth range of 100–400 km (table 3). To further constrain the anomalous domain we then analysed a large set of three-layer models. Two of these (with variance improvements 53% and 63% respectively) are shown in figure 10, which show that the high velocity anomaly decreases both in magnitude and areal extent for the layer 0–100 km compared with that for the layer 0–150 km. Significantly, the anomaly remains unaltered for depths of 400 km. In order to further test that the anomalies exposed by the above models are not an artefact of the choice of the number of layers, we also tested a suite of 4 layered models for inverting the travel time residuals. Figure 11 and table 4 show the model with various layers lying between 0 and 40 km, 40 and 200 km, 200 and 400 km and 400 and 600 km (variance improvement 46%). These models show that the high velocity anomaly is confined to layers 2 and 3 in the depth range of 40–400 km. As the depth to the top of the anomaly is reasonably well-constrained by the models (figure 10) described earlier we conclude that the high velocity anomaly coinciding with the southern two-thirds of the DVP exists in the depth range of 100–400 km. The 400–600 km layer is characterized by the presence of a very diffused low velocity and is distinct from the overlying layers. Table 4 shows

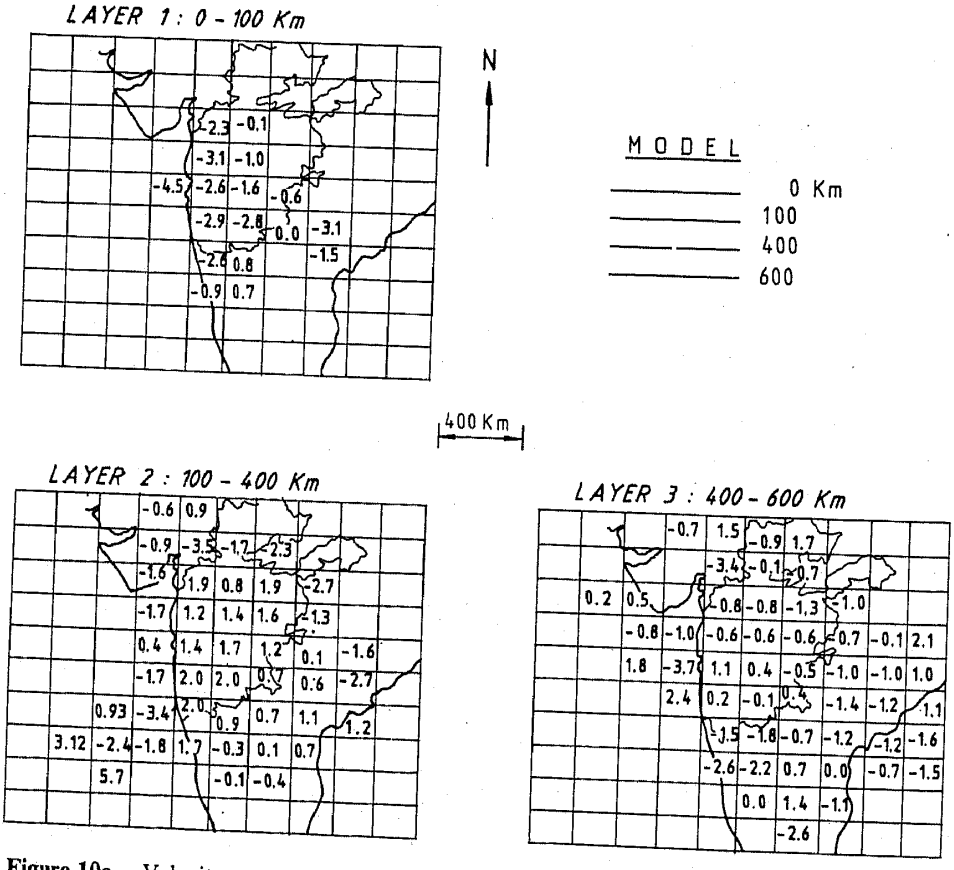

Figure 10a. Velocity perturbations in the three layers (0–100, 100–400, 400–600 km).

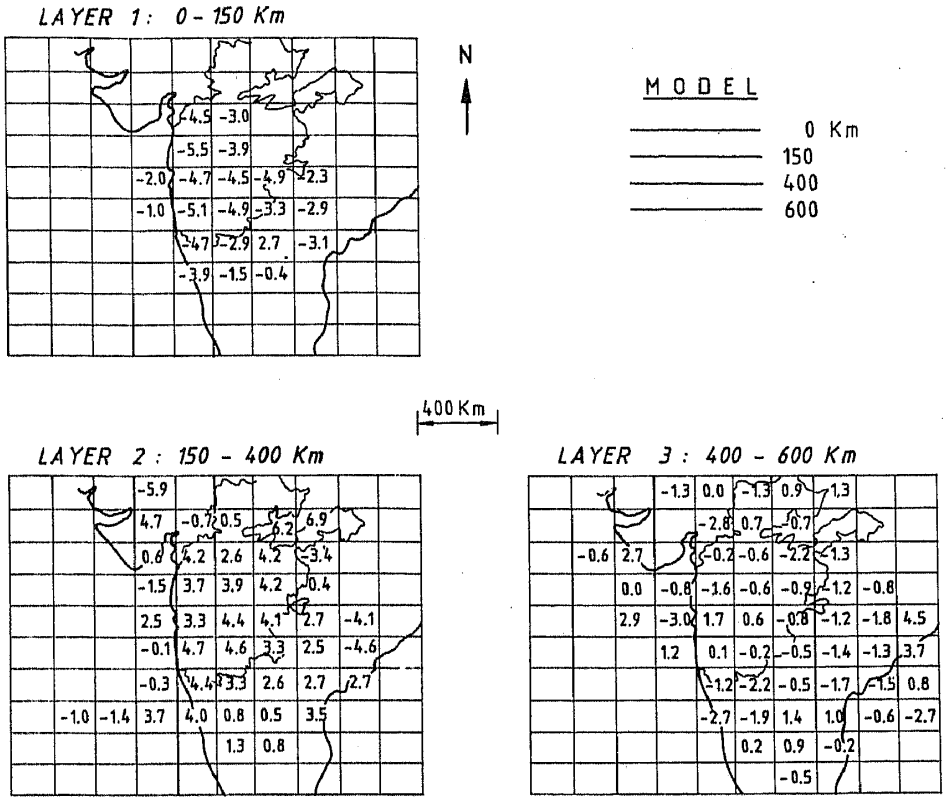

Figure 10b. Velocity perturbations in the three layers (0–150, 150–400, 400–600 km).

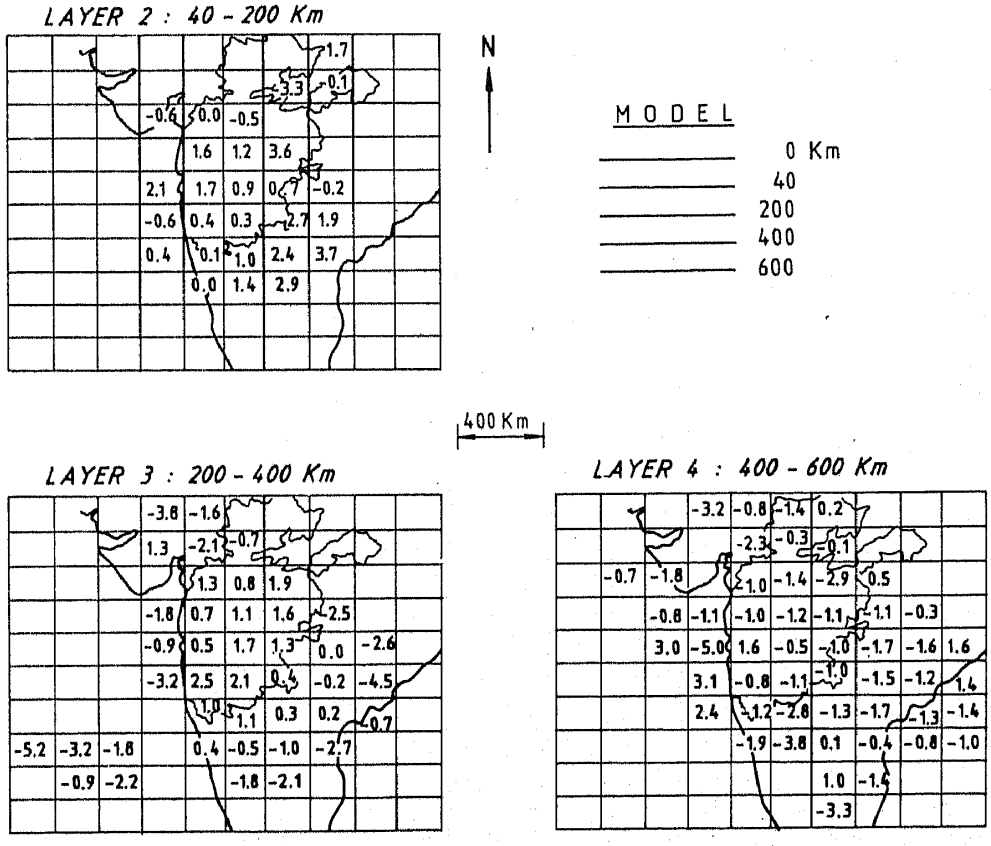

Figure 11. Velocity perturbations in the three sub-crustal layers of four-layer models.

Table 4. Full three-dimensional inversion for the four-layer model.

—up=N OW—

Layer 1

HYB 1	DHL 2	AUB 3	BIR 4	LTR 5	POO 6	GUL 7	SOP 8		
−3·16	−2·08	−1·81	−0·66	−2·37	−5·10	−7·14	−0·12		
182	17	39	41	46	112	29	36		
0·9114	0·9188	0·9421	0·9539	0·9543	0·9464	0·9194	0·9421		
2·55	2·76	2·16	1·81	1·78	1·90	2·51	2·08		
UJN 9	BHA 10	SAT 11	KOP 12	DWR 13	HPT 14	SLM 15	MPU 16		
−2·68	−5·57	−2·63	−1·10	−2·20	1·56	−8·67	−7·25		
30	27	75	73	59	73	12	21		
0·9522	0·9159	0·9369	0·9331	0·9143	0·8996	0·7747	0·9450		
1·80	2·56	2·04	2·05	2·43	2·71	4·15	2·02		

Layer 2

17	18	19	20	21	22	23	24	25	26
0	0	1	1	0	0	2	1·66 5 0·9804 1·50	3	0
27	28	29	30	31	32	33	34	35	36
0	0	0	3	2	1	−3·30 5 0·9557 2·19	−0·12 5 0·9657 1·94	2	0
37	38	39	40	41	42	43	44	45	46
0	0	1	−0·61 6 0·9765 1·53	0·00 22 0·9859 1·20	−0·54 13 0·9772 1·52	3	3	0	0
47	48	49	50	51	52	53	54	55	56
0	0	0	3	1·58 58 0·9904 0·93	1·22 78 0·9922 0·86	3·55 6 0·9501 2·35	3	0	1

57	58	59	60	61	62	63	64	65	66
			2·08	1·72	0·88	0·65	−0·28		
0	0	0	11	166	118	49	21	2	0
			0·9652	0·9916	0·9942	0·9913	0·9831		
			1·95	0·86	0·70	0·91	1·27		
67	68	69	70	71	72	73	74	75	76
			−0·55	0·44	0·32	2·69	1·91		
0	0	1	9	117	80	204	136	0	0
			0·9678	0·9908	0·9927	0·9891	0·9835		
			1·80	0·87	0·80	0·99	1·23		
77	78	79	80	81	82	83	84	85	86
			0·38	0·13	1·01	2·40	3·71		
0	0	4	6	66	93	22	15	0	0
			0·9718	0·9893	0·9879	0·9838	0·9689		
			1·73	0·94	1·01	1·28	1·60		
87	88	89	90	91	92	93	94	95	96
				−0·04	1·43	2·91			
0	0	0	2	7	66	28	0	0	0
				0·9759	0·9815	0·9752			
				1·53	1·29	1·54			
97	98	99	100	101	102	103	104	105	106
0	0	0	0	0	2	2	0	0	0
107	108	109	110	111	112	113	114	115	116
0	0	0	0	0	0	0	0	0	0
				Layer 3					
117	118	119	120	121	122	123	124	125	126
			−3·78	−1·64					
0	1	4	16	6	2	0	1	0	0
			0·9828	0·9726					
			1·40	1·77					

(continued)

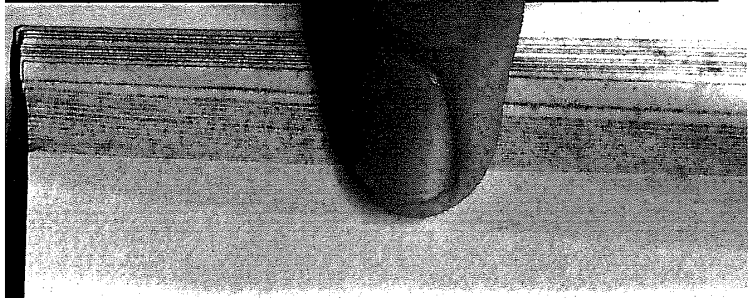

Table 4. (*continued*)

127	128	129	130	131	132	133	134	135	136
			1·28	−2·14	−0·71				
0	0	1	15	29	16	3	0	0	0
			0·9755	0·9844	0·9903				
			1·67	1·33	1·05				
137	138	139	140	141	142	143	144	145	146
				1·32	0·75	1·92			
0	0	2	0	39	40	17	4	0	1
				0·9926	0·9916	0·9894			
				0·91	0·98	1·10			
147	148	149	150	151	152	153	154	155	156
			−1·82	0·67	1·13	1·60	−2·49		
0	0	4	7	62	102	51	7	2	3
			0·8625	0·9940	0·9956	0·9944	0·9920		
			2·76	0·82	0·69	0·79	0·96		
157	158	159	160	161	162	163	164	165	166
			−0·90	0·52	1·72	1·29	−0·04	−2·64	
0	0	2	8	115	135	86	59	9	1
			0·9405	0·9940	0·9953	0·9955	0·9949	0·9796	
			2·11	0·81	0·70	0·70	0·75	1·50	
167	168	169	170	171	172	173	174	175	176
			−3·19	2·50	2·12	0·35	−0·17	−4·51	
0	0	1	7	45	103	75	132	41	0
			0·9784	0·9933	0·9952	0·9947	0·9943	0·9657	
			1·55	0·86	0·71	0·76	0·80	1·89	
177	178	179	180	181	182	183	184	185	186
				1·01	1·06	0·26	0·16	−0·66	
1	3	4	3	16	63	39	31	21	0
				0·9860	0·9942	0·9933	0·9886	0·9354	
				1·26	0·79	0·85	1·14	2·52	

187	188	189	190	191	192	193	194	195	196
−0·52	−0·32	−1·78		0·37	−0·46	−1·02	−2·72		
5	5	8	4	8	31	41	12	3	2
0·9712	0·9271	0·9619		0·9824	0·9868	0·9879	0·9556		
1·73	2·68	2·07		1·39	1·21	1·15	2·11		
197	198	199	200	201	202	203	204	205	206
	−0·90	2·15			−1·75	−2·08			
2	6	5	1	2	5	7	4	1	0
					0·9842	0·9466			
					1·33	2·41			
207	208	209	210	211	212	213	214	215	216
0	3	1	0	0	0	4	0	0	0

Layer 4

217	218	219	220	221	222	223	224	225	226
			−3·22	−0·80	−1·37	0·17			
0	0	1	6	28	22	6	3	1	1
			0·9694	0·9887	0·9927	0·9665			
			1·86	1·13	0·92	−0·25			
227	228	229	230	231	232	233	234	235	236
				−2·33	−0·32	−0·14			
4	2	0	1	24	25	15	2	3	0
				0·9895	0·9944	0·9864			
				1·10	0·80	1·26			
237	238	239	240	241	242	243	244	245	246
	−0·69	−1·77		−0·97	−1·36	−2·85	0·47		
2	6	5	1	19	42	30	8	3	4
	0·9773	0·6567		0·9914	0·9954	0·9953	0·9775		
	1·58	4·30		0·99	0·71	0·73	1·62		
247	248	249	250	251	252	253	254	255	256
		−0·78	−1·10	−0·99	−1·24	−1·12	−1·17	−0·32	

(*continued*)

Table 4. (*continued*)

0	2	9	6	19	74	66	32	26	4
		0·8991	0·9581	0·9943	0·9966	0·9967	0·9944	0·9885	
		2·56	2·15	0·80	0·60	0·60	0·80	1·15	
257	258	259	260	261	262	263	264	265	266
		3·03	−5·01	1·62	−0·50	−1·05	−1·72	−1·61	1·62
0	0	8	12	20	87	80	73	42	7
		0·9716	0·9770	0·9906	0·9958	0·9966	0·9970	0·9956	0·9733
		1·78	1·61	1·03	0·67	0·61	0·58	0·70	1·71
267	268	269	270	271	272	273	274	275	276
			3·12	−0·83	−1·09	−1·04	−1·53	−1·16	1·37
0	0	0	5	9	75	117	73	73	11
			0·9434	0·9898	0·9953	0·9968	0·9966	0·9935	0·9635
			2·51	1·08	0·72	0·58	0·62	0·86	1·97
277	278	279	280	281	282	283	284	285	286
			2·39	−1·17	−2·86	−1·32	−1·71	−1·26	−1·41
0	0	4	5	7	37	64	36	50	25
			0·9797	0·9791	0·9912	0·9956	0·9955	0·9950	0·9404
			1·53	1·55	0·99	0·70	0·71	0·76	2·52
287	288	289	290	291	292	293	294	295	296
				−1·91	−3·84	0·08	−0·45	−0·79	−1·01
0	2	3	3	6	12	32	34	12	8
				0·9713	0·9764	0·9931	0·9929	0·9564	0·9159
				1·80	1·64	0·88	0·90	1·76	2·96
297	298	299	300	301	302	303	304	305	306
						0·99	−1·36		
2	2	0	3	3	4	9	6	3	4
						0·9832	0·9837		
						1·39	1·36		
307	308	309	310	311	312	313	314	315	316
						−3·34			
0	0	1	1	3	3	5	2	4	2
						0·9724			
						1·77			

the diagonal elements of the resolution matrix along with the standard errors for this 4-layer model.

10. Interpretation

Existence of large-scale velocity anomalies in the upper mantle no longer evokes any surprise. Regional studies of one-dimensional velocity structure using travel-times, synthetic seismograms, and surface-wave dispersion, show that heterogeneous structure of the upper mantle is a rule rather than an exception in almost any region where observations are available. Teleseismic-residual studies show that velocity anomalies with dimensions of a few tens to a few hundreds of kilometers exist in the crust and upper mantle in North America and also in many other regions of the world (Aki 1982; Iyer 1984, 1988a, b; Thurber and Aki 1987; Iyer and Hitchcock 1988). In general, low-velocity anomalies are easier to interpret than high-velocity anomalies as the former seem to be generally associated with regions of young volcanism or recent orogeny. Some typical examples are: the Yellowstone hot spot (Iyer *et al* 1981); Rio Grande Rift (Parker *et al* 1984); Imperial Valley Spreading Centre (Humphreys *et al* 1984); Eastern U.S. (Taylor and Toksoz 1979); the Rhinegraben (Raikes and Bonjer 1983); and the Tarbela Area of Lesser Himalaya (Menke 1977). Higher-than-normal velocities, invariably found in active subduction zones and paleo-subduction zones are also reasonably well understood as they delineate subducting plates (for e.g., Japan: Hirahara 1981; Carapathian Arc: Romania: Oncescu *et al* 1984). Other high-velocity anomalies, not so well understood, are found in the upper mantle beneath the Baltic Shield (Husebye and Hovland 1982); Eastern Senegal, West Africa (Dorbath *et al* 1983); the Alps (Baer 1980); the North China Basin (Shedlock and Roecker 1987); the Timber Mountain Caldera Complex, Nevada (Evans and Oliver 1987); and the Southern Sierra Nevada, California (Humphreys *et al* 1984; Humphreys 1987), to name a few. Humphreys (1987) interprets the vertical, tongue-shaped, high-velocity anomaly extending to depths of 300–400 km in Sierra Nevada, as representing a descending sub-crustal lithosphere caused by small-scale convection. Available case histories on large-scale high-velocity anomalies, though similar in size and velocity contrast, are simply too few to allow any detailed comparisons with the anomaly which we have delineated beneath the DVP.

A fundamental question to be addressed regarding the DVP anomaly is the following. Is the anomaly at all related to the Deccan volcanism or is it simply an integral part of the architecture of the upper mantle of the Indian shield? There is enough evidence from global and continental scale geophysical data to show that old continents are indeed far from being homogeneous in their deep crust and upper mantle structure. Our modelling results lead to startling revelations indicating the presence of an anomalously thick high-velocity region beneath the DVP. The presence of such an anomaly at depths much greater than the conventionally accepted plate thickness (of about 100–200 km) could be best explained in the light of the concept of continental tectosphere (Jordan 1975, 1979a, b) and stabilization of cratons (Pollack 1986). The existence of lithospheric roots to depths as great as 400 km has been inferred earlier in Western North America, Superior Province of Canada and South Africa based on petrological, geothermal and seismological investigations (Grand and Helmberger 1984; Pollack 1986; Lam and Jordan 1987; Silver and Chan 1988). The

tectosphere is proposed to be a region of massive basalt depletion and is predominantly composed of olivine and orthopyroxene, resulting in a density reduction of 1% and an increase in *S*-wave velocity due to lowering of the iron content. To constrain the density of the anomalous region beneath the DVP, we analysed two gravity profiles (west to east and north to south) taken from the 5 mgal contour Bouguer gravity anomaly map of India. These indicate the presence of a long wavelength, 35 mgal gravity low present over the region of high-velocity anomaly. A preliminary inversion of the data delineates the lower density region roughly lying within the high velocity anomalous region in the depth range of 100–300 km, with a density contrast of about −0·006 to −0·013 grams per cc (D Srinagesh, personal communication).

The other line of evidence is from *S*-wave residuals at POO relative to HYB taken from ISC catalogues (figure 12). In spite of the poor quality of data and consequent high scatter, it is quite obvious that we see an azimuthal pattern broadly similar to that shown by *P*-wave residuals at POO. The *S*-residuals are about three times as large as the corresponding *P*-wave residuals shown alongside for comparison. Shear wave structure beneath the DVP delineated by Montagner (1986) using surface wave data also reveals the existence of a high-velocity anomalous zone in the depth range of 85–250 km. However, the continuation of this anomaly beyond 250 km depth is not observed due to data constraints in the surface wave study.

11. Source of Deccan basalts

Let us now consider the question of the source of Deccan basalts in the light of the existence of a deep continental root under this region, which must have acquired a coherent stable structure long before the Gondwanaland break-up considering that the craton came into existence earlier than at least 2·5 billion years. The formation of tectosphere due to the depletion of volatiles which elevates the solidus, renders the upper mantle region more resistant to subsequent melting. Such stable regions are observed to have normal shield heat flow values (Pollack 1986). This is in conformity with the observed normal heat flow over DVP (Gupta and Gaur 1984). The very presence of the tectosphere beneath the DVP would therefore inhibit the development of large scale perforations which are believed to have been responsible for the extrusion of such extensive flood basalts, implying the absence of their source region directly beneath the DVP. On the other hand, it is significant to note that in all the models, the per cent velocity anomaly beneath the westernmost part of the DVP in the depth range of 40–200 km is relatively less than that observed in other parts. This is also reflected in the results of surface wave study (Nataf *et al* 1984) showing a regional low shear wave velocity enveloping the entire Arabian Sea extending from the east coast of Africa to the west coat of India. However, it is significant to observe that the above low velocity zone is confined to the west of our westernmost profile 2.

Also, recent studies of major and trace element abundances and inter-element ratios as well as Sr isotopic ratios in selected samples combined with extensive field checks in the western parts of the DVP show that the flow sections do not correspond to a classical layer cake-sequence. Instead, they appear to be comprised of a sequence of thicker and older formations in the north which become thinner in the south and are superceded by southward thickening of younger ones that taper out further southwards. This interlocking sequence strongly suggests that the flows are derived

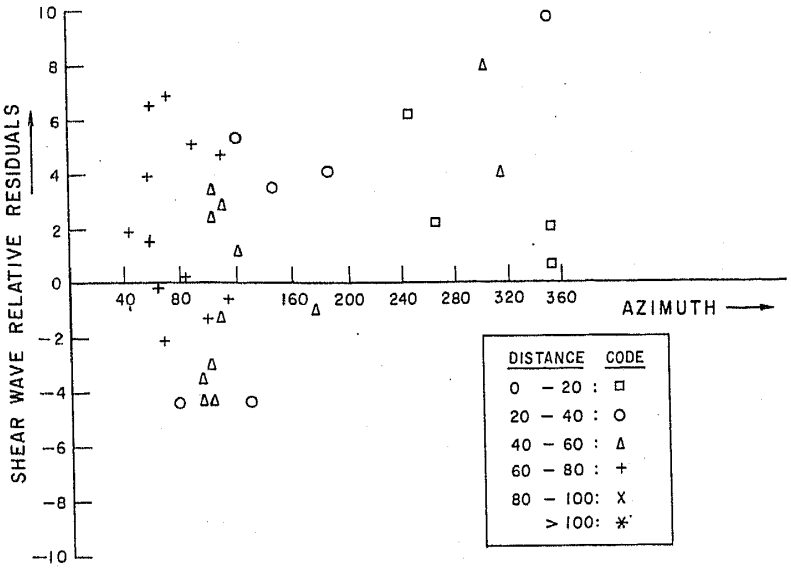

RELATIVE SHEAR WAVE TRAVEL TIME RESIDUALS
AT POONA WITH RESPECT TO HYDERABAD

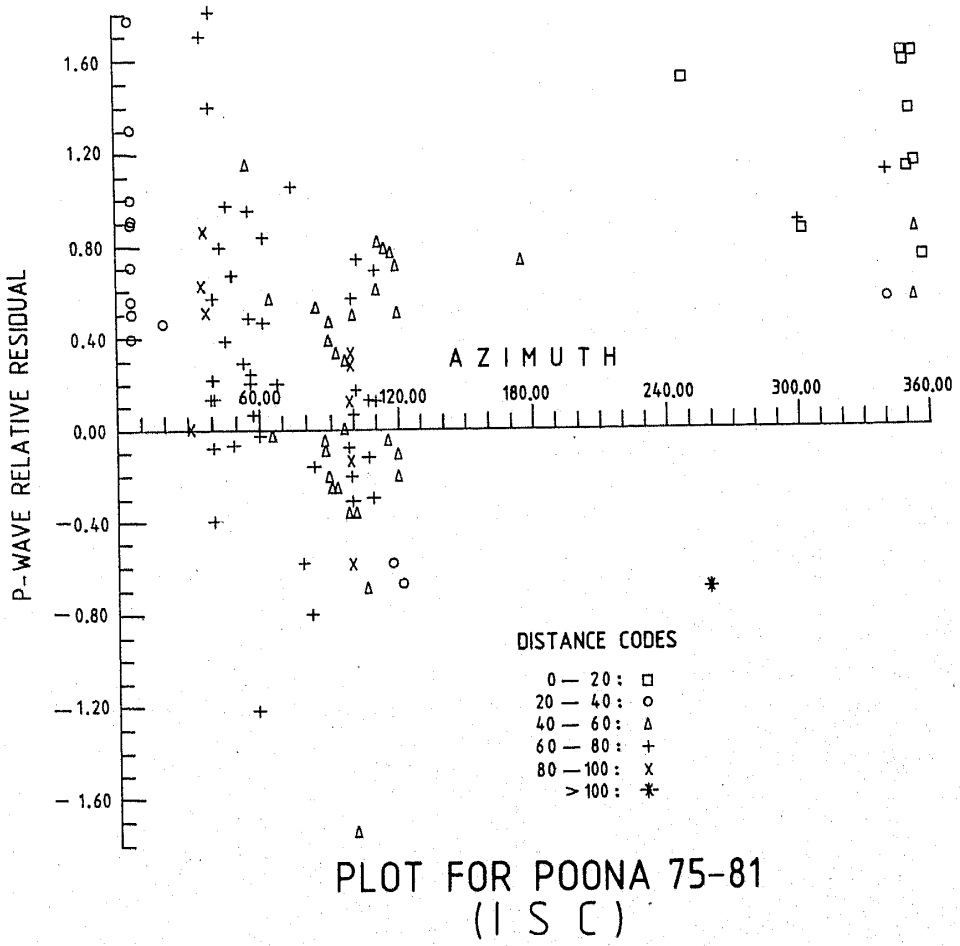

Figure 12. Typical azimuthal variation of *P* and *S*-wave relative residuals at POO with respect to HYB compiled from the International Seismological Summary catalog.

from southward migration of a centre of magmatic egress rather than from a system of fissures tapping the lower crust or upper mantle directly beneath the DVP. Further, Nd and Sr isotopic values of least contaminated Deccan Tholeiites from different areas of the DVP fall in a restricted field of high ε_{Nd} which closely approach those of old and present-day Central Indian ridge basalts. This strongly suggests that the Deccan basalts were derived from the same large region of isotopically homogeneous oceanic mantle (Mahoney 1988) which feeds the Central Indian ridge. Considering further that the bulk of Deccan basalts were formed about 65 Ma ago shortly after the rifting between India and Madagascar (80 Ma) when the ridge axis jumped towards India (Norton and Sclater 1979; Schlich 1982), a more natural channel for their outpouring would appear to be associated with the rift systems that eventually fashioned the Indian west coast passive continental margin. If the above visualization of the formation of Deccan basalts is correct, we should expect to see a low velocity zone (LVZ) on the western periphery of the DVP representing the source of the Deccan basalts perhaps characterized by high heat flow values but no thermal anomaly over the DVP. While the heat flow over the LVZ still remains to be measured, the other two predictions from the model are indeed confirmed by observational evidence.

12. Conclusions

Using teleseismic *P*-wave residual tomography, we have identified a large region in the upper mantle beneath the Deccan volcanic province in which the *P*-wave velocity is higher than that in the surrounding region by 1 to 4%. This high velocity anomaly exists coherently in the depth range of 100–400 km. This implies that a coherent, colder and comparatively rigid lithospheric root extends to a depth of about 400 km beneath the DVP. The anomaly in the depth range of 400–600 km is distinctly weaker and appears to be decoupled from the overlying layers. This is as we expect owing to diminished ability of the asthenosphere to retain heterogeneities over extended periods of geologic times. Persistence of the anomaly in the upper mantle is however maintained through a stable geochemical reordering and formation of a tectosphere beneath the craton which together translate coherently over the underlying weaker mantle.

Acknowledgements

Support for this work came from three organizations: the Indo-US Subcommission on Education and Culture which awarded a fellowship to Iyer to spend 13 months in India; the National Geophysical Research Institute which provided full research support; and the U.S. Geological Survey which permitted Iyer's visit to India and completion of the research on his return to USA. Special thanks are due to the Director and staff of the Indian Institute of American Studies, New Delhi for efficiently managing Iyer's fellowship and assisting him in innumerable ways. We are greatly indebted to the various universities, colleges and many individuals for the warm cooperation extended to us in running our field stations during this work. We are very grateful to these organisations and also to many field assistants from NGRI, who participated in the experiment, to Phil Dawson for extensive support in data

analysis and to Tim Hitchcock and M Jayarama Rao for help throughout the project including preparation of figures for this manuscript. Grateful thanks are also due to M/s. N K Venkatesh and G Ramakrishna Rao for the excellent typing of the manuscript.

References

Achauer U, Greene L, Evans J R and Iyer H M 1986 Nature of magma chamber underlying the Mono craters area, eastern California, as determined from teleseismic travel time residuals; *J. Geophys. Res.* **91** 13872–13891

Aki K 1982 Three-dimensional seismic inhomogeneities in the lithosphere and asthenospehre: evidence for decoupling in the lithosphere and flow in the asthenosphere; *Rev. Geophys. Space Phys.* **20** 161–170

Aki K, Christoffersson A and Husebeye E S 1927 Determination of the three-dimensional seismic structure of the lithosphere; *J. Geophys. Res.* **82** 277–296

Baer M 1980 Relative travel time residuals for teleseismic events at the new Swiss seismic station network; *Ann. Geophys.* **36** 119–126

Dorbath C, Dorbath L, Le page A and Gaulon R 1983 The West-African craton margin in eastern Senegal; a seismological study; *Ann. Geophys.* **1** 25–36

Ellsworth W L and Koyanagi R Y 1977 Three-dimensional crust and mantle structure of Kilanea Volcano, Hawaii; *J. Geophys. Res.* **82** 5379–5394

Evans J R 1982 Compressional wave velocity structure of the upper 350 km under the eastern Snake River Plain near Rexburg, Idaho; *J. Geophys. Res.* **87** 2654–2670

Evans J R and Oliver H W 1987 Comparison of Timber Mountain caldera complex, Nevada, with Yellowstone; speculations on mechanisms (Abs), Abstract Volume; *Hawaii Symposium on How Volcanoes Work* (Hilo, Hawaii: Hawaiian Volcano Observatory) p. 67

Grand S P and Helmberger D 1984 Upper mantle shear structure of North America; *Geophys. J. R. Astron. Soc.* **76** 399–438

Gupta M L and Gaur V K 1984 Surface heat flow and probable evolution of Deccan volcanism; *Tectonophysics* **105** 309–318

Hirahara K 1981 Three-dimensional seismic structure beneath southwest Japan: the subducting-phillippine sea plate; *Tectonophysics* **79** 1–44

Herrin E 1968a Seismological tables for *P*; *Seismol. Soc. Am. Bull.* **58** 1193–1241

Herrin E 1968b *P*-wave velocity distribution in the mantle; *Seismol. Soc. Am. Bull.* **58** 1223–1225

Humphreys E 1987 Mantle dynamics of the southern Great Basin-Sierra Nevada region (Abs); *EOS Trans. Am. Geophys Union* **68** 1450

Humphreys E and Clayton R W 1988 Adaptation of back-projection tomography to seismic travel time problems; *J. Geophys. Res.* **93** 1073–1085

Humphreys E, Clayton R W and Hager B H 1984 A tomographic image of mantle structure beneath southern California; *Geophys. Res. Lett.* **11** 625–627

Husebye E S and Hovland J 1982 On upper mantle seismic heterogeneities beneath Fennoscandia; *Tectonophysics* **90** 1–17

Iyer H M 1984 Geophysical evidence for the locations, shapes and sizes, and internal structures of magma chambers beneath regions of Quaternary volcanism. In *Relative contributions of mantle, oceanic crust, and continental crust to magma genesis*, (eds) S Moorbath, R N Thompson and E R Oxburg (Philos Trans. R. Soc. London) **A310** 473–510

Iyer H M 1988a *Seismic tomographys. Encyclopedia of geophysics* (ed.) D James, (Van Nostrand Reinhold and Co.) (in press)

Iyer H M 1988b Seismological detection and delineation of magma chambers beneath intraplate volcanic centres in western USA. In *Modelling volcanic processes* (eds) C King and R Scaroa (Braunschweig/ Wiesbaden: Friedr. Vieweg and Sohn) pp. 1–56

Iyer H M, Evans J R, Zandt G, Stewart R M, Coakley J M and Roloff J N 1981 A deep low-velocity body under the Yellowstone caldera, Wyoming: delineation using teleseismic *P*-wave residuals and tectonic interpretation; *Geol. Soc. Am. Bull.* **92** Part I (Summary), 792–798; part II (full text in microfische edition) 1471–1646

Iyer H M and Hitchcock T 1988 Upper mantle velocity structure in continental US and Canada. Geophysical framework of the Continental United States; *Geol.* Soc. *Am. Mem.* (in Press)

Jordan T H 1975 The continental tectosphere; *Rev. Geophys. Space Phys.* **13** 1–12

Jordan T H 1979a Lateral heterogeneity and mantle dynamics; *Nature (London)* **257** 745–750

Jordan T H 1979b The deep structure of continents; *Sci. Am.* **240** 92–107

Kaila K L 1982 Deep seismic sounding studies in India; *Geophys. Res. Bull. NGRI, India* (Special Issue) **20** 309–328

Kaila K L, Tewari H C and Sarma, P L N 1981 Crustal structure from deep seismic sounding studies along Navibandar-Amreli profile in Saurashtra, India. In *Deccan volcanism and related basalt provinces in other parts of the world* (eds) K V Subba Rao and R N Sukheswala, Geol. Soc. India Memoir No. 3 pp. 218–232

Kaila K L, Reddy P R, Dixit M M and Koteswara Rao P 1985 Crustal structure across the Narmada-Son lineament, Central India from deep seismic soundings; *J. Geol. Soc. India* **26** 465–480

Kailasam L N 1975 Epirogenic studies in India with reference to recent vertical movements; *Tectonophysics* **29** 505–521

Lam A L L and Jordan T H 1987 How thick are the continents; *J. Geophys. Res.* **92** 14007–14026

Mahoney J J 1988 Deccan basalts. In *continental flood basalts* (ed.) J D Macdougall (Kluiser, Norwell, MA)

Menke W H 1977 Lateral inhomogeneities in *P* velocity under the Tarbela array of the lesser Himalayas of Pakistan; *Bull. Seismol. Soc. Am.* **67** 725–734

Montagner J P 1986 Regional three-dimensional structures using long period surface waves; *Ann. Geophys.* **4** 283–294

Morgan W J 1972 Deep mantle convection plumes and plate motions; *Bull. Am. Assoc. Petrol Geol.* **56** 203–213

Nataf H C, Nakanishi I and Anderson D L 1984 Anisotrophy and shear-velocity heterogeneities in the upper mantle; *Geophys. Res. Lett.* **11** 109–112

Norton I O and Sclater J G 1979 A model for evolution of the Indian Ocean and break-up of Gondwanaland; *J. Geophys. Res.* **84** 6803–6830

Oncescu M C, Burlacu V, Anghel M and Smalbergher V 1984 Three-dimensional *p*-wave velocity image under the Carpathinan Arc; *Tectonophysics* **106** 305–319

Parker E C, Davis P M, Evans J R, Iyer H M and Olsen K H 1984 Upwarp of anomalous asthenosphere beneath the Rio qrande rift; *Nature (London)* **312** 354–356

Pollack H N 1986 Cratonization and thermal evolution of the mantle; *Earth. Planet. Sci. Lett.*, **80** 175–182

Qureshy M N 1981 Gravity anomalies, isostasy and crust mantle relations in the Deccan Trap and contiguous regions, India. In *Deccan volcanism and related baslt provinces in other parts of the world* (eds) K V Subba Rao and R N Sukheswala, Geol. Soc. India Memoir No. 3 185–197

Raikes S and Bonjer K P 1983 Large-scale mantle heterogeneity beneath the Rheinish Massif and its vicinity from teleseismic *p*-residuals measurements. In *Plateau uplift* (eds) K Fuchs *et al* (Berlin Heidelberg: Springer-Verlag) 315–331

Shedlock K M and Roecker S W 1987 Elastic wave velocity structure of the crust and upper mantle beneath the North China Basin; *J. Geophys. Res.* **92** 9327–9350

Schlich R 1982 The Indian Ocean: Aseismic ridges, spreading centres, and oceanic basins. In *The oceans basins and margins, Vol. 6 The Indian Ocean* (eds) A E M Nairn and F G Stelhi (New York: Plenum Press) 51–147

Silver P G and Chan W W 1988 Implications for continental structure and evolution from seismic anisotropy; *Nature (London)* **335** 34–39

Takin M 1966 An interpretation of the positive gravity anomaly over Bombay on the west coast of India; *Geophys. J. R. Astron. Soc.* **11** 527–537

Taylor S R and Toksoz M N 1979 Three-dimensional crust and upper mantle structure of the northern United States; *J. Geophys. Res.* **84** 7627–7644

Thurber C H and Aki K 1987 Three-dimensional seismic imaging; *Ann. Rev. Earth Planet. Sci.* **15** 115–139